JOURNAL OF MATERIALS SCIENCE 39 (2004) 4615–4623

# Synthesis and characterization of polyurethane/polybutyl methacrylate interpenetrating polymer networks

MUNEERA BEGUM*, SIDDARAMAIAH‡
*Department of *Chemistry and ‡Polymer Science & Technology, S.J. College of Engineering, Mysore 570 006, India*
*E-mail: siddaramaiah@yahoo.com*

A series of castor oil based polyurethane (PU) and poly (butyl methacrylate) (PBMA) interpenetrating polymer networks (IPNs) (PU/PBMA; 80/20, 60/40, 50/50, 40/60 and 20/80) were prepared by sequential polymerization method using toluene diisocyanate (TDI), dibutyl tin dilaurate (DBTL) as catalyst and ethylene glycol dimethacrylate (EGDM) as crosslinker. Tensile strength, percentage elongation at break and surface hardness; FTIR and optical properties of the IPNs are reported. Thermo gravimetric analyzer (TGA) studies of the IPNs are performed in order to establish their thermal stability. TGA thermogram shows that the thermal degradation of IPN was found to proceed in three steps. The microcrystalline parameters such as crystal size ($\langle N \rangle$) and lattice disorder ($g$ in%) of IPNs have been estimated using wide angle X-ray scattering (WAXS) studies. The surface morphology of the IPNs has been studied using scanning electron microscope (SEM).


## 1. Introduction

The use of renewable resources has attracted the attention of many researchers, due to their potential as substitutes for petrochemical derivatives. Much attention has been focused on the innovation and development of newer materials from renewable resources, i.e., forest products that could be grown again and again. One of the most naturally and abundantly occurring vegetable oil is castor oil. Castor oil possesses both unsaturation and conjugated hydroxyl functional groups. Castor oil reacts with different diisocyanate which is also polyfunctional to form a prepolymer called prepolyurethane (PU) [1–3]. Pre-polyurethanes are linear block co-polymers in which one of the two blocks is typically a polyether or a polyester diol. These blocks comprise the soft segments because at the service temperature they exist in rubbery or viscous state and impart elastomeric properties. The presence of these segments shows their dimensional stability imparted through microphase separation. A wide range of physical and morphological properties can be obtained, depending upon the composition and chemical structure of the hard and soft segment.

The synthesis of interpenetrating polymer networks (IPNs) is a useful technique for designing materials with a wide variety of properties. IPNs generally possess enhanced physico-mechanical properties against the normal polyblends of their components. IPNs could also be called polymer alloys and they are considered to be one of the fastest growing areas of polymer blends during the last two decades. Recently, IPNs derived from castor oil have gained wide spread acceptance in industrial applications and newer IPNs showing better applications are emerging day by day. Sperling and co-workers have reported the synthesis and characterization of IPNs from various natural products [4–10]. Recently we have reported [11–13] the properties of some IPNs derived from castor oil.

PU is a versatile polymer with unique chemistry, excellent mechanical and optical properties and has good solvent and oil resistance, but lacks of low temperature stability, whereas butyl methacrylate (BMA) has excellent solvent and oil resistance, low temperature properties, optical behaviour and excellent adhesive nature. Thus, an IPN of these two polymers is likely to produce a material having excellent mechanical properties, solvent and oil resistance properties. This research article deals with the physico-mechanical, optical, thermal properties, microcrystalline parameters and morphological behaviour of castor oil with TDI based PU/PBMA IPNs.

## 2. Experimental

### 2.1. Materials

Castor oil was obtained from local market and its characteristic values such as hydroxyl number (160–190), acid number (1.48) and isocyanate equivalent (330) were determined as per standard procedure [7]. The other chemicals like toluene diisocyanate (TDI) and benzoyl peroxide (BPO) (Aldrich, USA) were used without further purification. Butyl

methacrylate (BMA) (E-Merck, Switzerland) was freed from stabilizer prior to use. Ethylene glycol dimethacrylate (EGDM) and dibutyl tin dilaurate (DBTL) (Fluka, Switzerland) were used without further purification.

## 2.2. Synthesis of PU/PBMA IPNs

A series of PU/PBMA IPNs (PU/PBMA; 80/20, 60/40, 50/50, 40/60 and 20/80) were synthesized by sequential polymerization method [6, 7]. The prepolyurethane was prepared by reacting hydroxyl groups of castor oil with TDI in the NCO/OH molar ratio of 1.4. This PU was swollen in a calculated amount of butyl methacrylate monomer and subsequently polymerized by free radical polymerization initiated with 0.5% benzoyl peroxide (BPO) in the presence of 1% ethylene glycol dimethacrylate (EGDM) as cross linker and 0.5% dibutyl tin dilaurate (DBTL) as catalyst. The mixture was stirred constantly at room temperature for 15 min to form a homogeneous solution. After stirring for one hour, the solution was poured into a cleaned glass mould sprayed with releasing agent. The mould was kept at room temperature for 24 h for PU polymerization.

The temperature of the mould was then slowly raised to 80°C to initiate butyl methacrylate (BMA) polymerization and kept for 10 h, followed by 10 h at 100°C. The golden yellow transparent and tough PU/PBMA IPN films thus formed were cooled slowly and removed from the mould with different compositions of PU and PBMA.

## 2.3. Physical and mechanical characterization

FTIR spectra for thin transparent films of PU/PBMA IPNs were recorded using Perkin Elmer IR-2000 instrument in the wave number range 4000–400 $cm^{-1}$. Density, surface hardness and resilience were measured as per ASTM D-792, ASTM D-785 and ASTM D 2632-88 respectively. Mechanical properties like tensile strength and percentage elongation at break were measured as per ASTM D-882 method using Hounsfield Universal testing machine (UTM) H50 KM, 50 kN at 27°C. A minimum of six samples were tested for each composition and the average value was reported. The optical properties of dust and grease free IPN [14] films were measured using Suga Test, Hazemeter (model 206, Japan) as per ASTM D-1003.

## 2.4. Thermogravimetric analyzer

The thermal analysis of the IPNs was carried out using a TG Metler Polymerchemic Marburg FB 14 instrument with thermogravimetric module. The TGA scans were taken in the temperature range 30–800°C at a heating rate of 20°C/min in nitrogen atmosphere.

The relative thermal stability of the PU/PBMA IPNs were evaluated by comparing decomposition temperatures at various percent weight losses and integral procedural decomposition temperature (IPDT). The IPDT is defined as a means of summing up of the whole shape of the normalized TGA data curve. IPDT is an index of thermal stability, was determined from the thermogram area using the method reported in the literature [15]. The oxidation index (OI) was calculated based upon the weight of carbonaceous char (CR) as related by the empirical equation;

$$\mathrm{OI} \times 100 = 17.5 \times 0.4\ \mathrm{CR} \tag{1}$$

## 2.5. X-ray powder pattern recording and analysis

X-ray powder pattern of IPNs were recorded using Philips PW 1140 diffractometer of Bragg-Branto Geometry (fine focus setting) with germanium mono chromated radiation of Co $K_\alpha$ ($\lambda = 0.179$ nm) for $2\theta$ range 5 to 50° at intervals of 0.03° employing a curved position sensitive detector (CPSD) in the transmission mode. These patterns were indexed using TREOR procedure. The intensity was corrected for Lorentz-polarization factors and also for instrumental broadening using Stokes' deconvolution method [16].

Each of the Bragg reflections in these samples, referred as (*hkl*) reflections, are broadened due to crystal imperfections. We have used profile analysis technique to quantify these imperfections. Normally, the broadening of the profile arises due to the limited number of unit cells $\langle N \rangle$ (a measure of crystal size), counted in a direction perpendicular to Bragg planes (*hkl*) and a disorder of second kind, referred to as lattice strain ($g$ in%). This is given by $\Delta d/d$, where $\Delta d$ is the change in the inter planar spacing and $d$ is the inter planar spacing.

It is possible to simulate an intensity profile using Hosemann's one-dimensional linear paracrystalline model and the equation used for this purpose is as following [17];

$$I(s) = I_{N-1}(s) + I'_N(s) \tag{2}$$

Here $s = (2\pi \sin(\theta)/\lambda)$ and '$N$' is the number of unit cells causing a Bragg reflection. Where, $I_{N-1}(s)$ is computed using;

$$I_N(s) = 2\mathrm{Re}[(1 - I^{N+1})/(1 - I) + I_v/D(1 - I)^2\{I^N(N(1 - I) + 1) - 1\}]^{-1} \tag{3}$$

with $v = 2ia^2s + d$, $I = I(s) = \exp(-a^2s^2 + ids)$ with $a^2 = \omega^2/2$ and $D = Nd$.

Here $I'_N(s)$ is the modified intensity for the probability peak centered at $D$. By substituting $D = dN$, we have

$$I'_N(s) = (2a_N/D\pi^{1/2}) \exp(iDs)\big[1 - a_N s\{2\, D(a_N s) + i/\pi^{1/2} \exp(-a_N^2 s^2)\}\big] \tag{4}$$

with $a_N^2 = N\omega^2/2$, $\omega$ is the standard deviation of the nearest neighbour probability function [18] and $D(a_N s)$ is Dawson's integral or the error function with purely complex argument and can be easily computed. $N$ is

the number of unit cells counted in a direction perpendicular to the ($hkl$) Bragg plane and $d$ is the spacing of the ($hkl$) planes. Re refers to the real part of the expression, $s$ is $\sin\theta/\lambda$, $\lambda$ is the wavelength of the X-ray used, $a$ is related to the standard deviation and $\omega$ is a lattice distribution function and $D$ is the crystal size ($= \langle N\rangle d_{\mathrm{hkl}}$). $I_{\mathrm{N}}(s)$ is the modified intensity for the probability peak centered at $D$. The experimental profile between $s_{\mathrm{o}}$ (peak) and $s_{\mathrm{o}} + s_{\mathrm{o}}/2$ (or $s_{\mathrm{o}}$ and $s_{\mathrm{o}} + B/2d$, if there is a truncation of the profile $B < 1$) is matched with corresponding simulated reflection profile between $s_{\mathrm{o}}$ and $s_{\mathrm{o}}/2$ (or $s_{\mathrm{o}}$ and $s_{\mathrm{o}} + B/2d$) using a one-dimensional para crystalline model for various values of $\langle N\rangle$ and $g$ to minimize the difference between calculated and experimental normalized intensity values. SIMPLEX, a multidimensional algorithm [18, 19] was used for minimization. The estimated enthalpy $\alpha\,(= N^{1/2}g)$ which physically implies that the growth of the para crystals in a particular material is appreciably controlled by the level of $g$ in the net plane structure. This is only an empirical definition if enthalpy is as given by Hosemann in order to characterize the materials.

From these values, the surface weighted ($D_{\mathrm{sur}}$) and volume weighted ($D_{\mathrm{vol}}$) crystal sizes were determined using the following integrals [20];

$$\langle D\rangle_{\mathrm{s,v}} = \frac{\int_0^\infty LP_{\mathrm{s,v}}(L)\mathrm{d}L}{\int_0^\infty P_{\mathrm{s,v}}(L)\mathrm{d}L} \tag{5}$$

where,

$$P_{\mathrm{s}}(L)\,\alpha\,[d^2A_{\mathrm{s}}(n)/\mathrm{d}L^2] \tag{6}$$

and

$$P_{\mathrm{v}}(L)\,\alpha\,L[d^2A_{\mathrm{s}}(n)/\mathrm{d}L^2]$$

where, $L = nd$ and $A_{\mathrm{s}}(n)$ is the size-Fourier coefficients, $n$ is the harmonic number and $d$ is the interplanar spacing [21].

### 2.6. Surface morphology

The surface morphology was studied using scanning electron microscopy (SEM). The micrographs of IPNs were taken using Leo-435 VP electron probe microanalyzer SX-50 with probe microanalysis Sl. 320 after gold (10 nm) coating. The planar views of the IPNs were scanned. The magnification value is displayed on the respective microphotographs.

## 3. Results and discussion

### 3.1. Fourier transform infrared spectroscopy (FTIR)

FTIR spectra of PU, PBMA and PU/PBMA IPNs are shown in Fig. 1a–c respectively. The FTIR spectra of both PU and PBMA are in good agreement with literature IR data [22, 23]. The FTIR spectrum of PU is

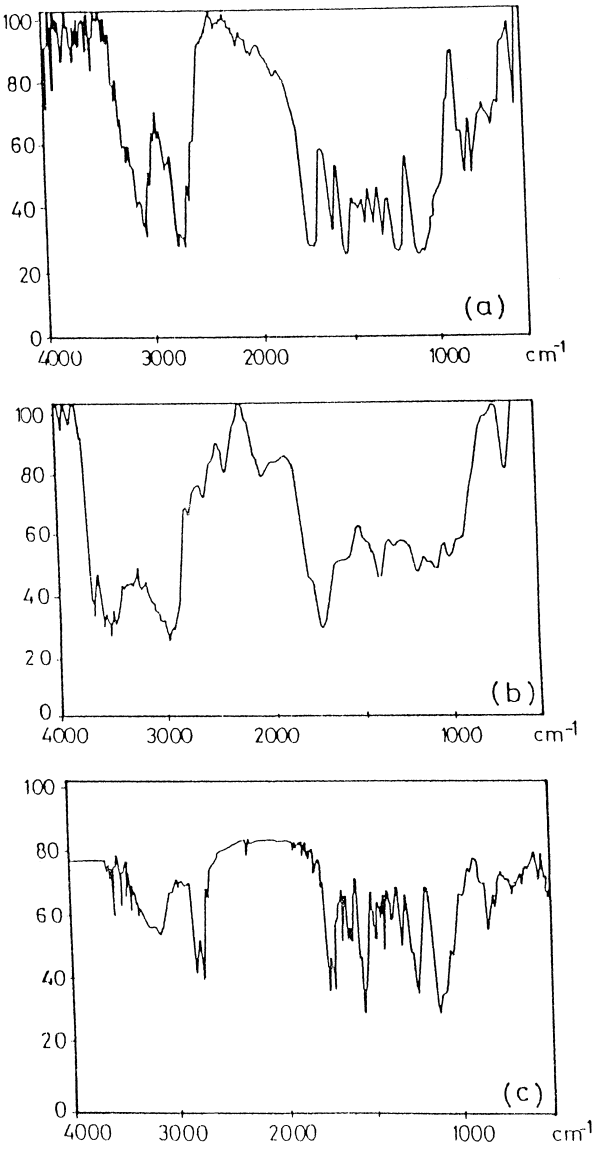


*Figure 1* FTIR spectra of: (a) PU, (b) PBMA and (c) PU/PBMA.

characterized by a very broad peak at 3400–3200 $\mathrm{cm}^{-1}$, due to the —NH stretching of the urethane linkage with finite contribution from extensive hydrogen bonding in the system. The free —NH stretching band occurs at approximately 3350 $\mathrm{cm}^{-1}$ and an intense sharp discremible band around 2264 $\mathrm{cm}^{-1}$ assigned to the isocyanate group, indicates that these polyurethanes are isocyanate terminated polymers.

The FTIR spectrum of PBMA is characterized by a very strong absorption peak at 1734 $\mathrm{cm}^{-1}$ which is due to —C=O stretching of the ester group (Fig. 1b). Another strong absorption peak at 1308 $\mathrm{cm}^{-1}$ may be attributed to C—O stretching of the methyl ester group accompanied by another strong absorption band around 1250 $\mathrm{cm}^{-1}$ which is due to $-OCH_3$ stretching of the methyl ester group. The presence of a peak at 1640 $\mathrm{cm}^{-1}$ indicates C=C stretching mode of the methacrylate moiety. The bands at 1112 and 800 $\mathrm{cm}^{-1}$ could be assigned to the in-plane and out of plane C—H bending modes respectively.

The IR spectrum of IPN shows a peak at 1600–1580 $\mathrm{cm}^{-1}$ which is due to the aromatic group (Fig. 1c). Theoretically, aromatic —CH gives a sharp doublet in

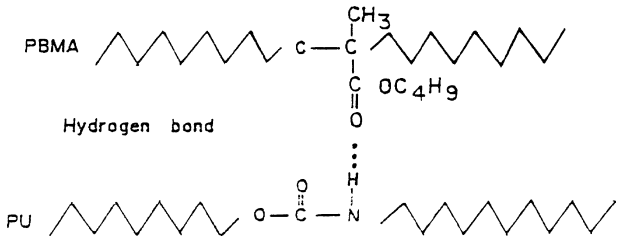


*Scheme 1* Schematic representation of hydrogen bond formation between PU and PBMA.

the range 3080–3010 $cm^{-1}$, whereas we observed one peak at 3025 and another at 3150 $cm^{-1}$. In the carbonyl stretching (1735 $cm^{-1}$) region of PU/PBMA, the observed frequency shift is 28 $cm^{-1}$, typically assigned to hydrogen bonded urethane carbonyls. The frequency band of the ester group at 1750 $cm^{-1}$ is assigned to the "free" carbonyls, the frequency band at 1723 $cm^{-1}$ could be attributed to hydrogen bonded ester carbonyls and/or of hydrogen bonded urethane carbonyls. Seymour *et al*. [24] concluded that all the –NH groups are involved in hydrogen bonding. The schematic representation for the hydrogen bond formation between PU and PBMA is shown in Scheme 1.

## 3.2. Physico-mechanical properties

All the IPNs are obtained as tough films, colored golden yellow to yellow. The physico-mechanical properties, including density, surface hardness, tensile strength, percentage elongation at break and tensile modulus of the PU/PBMA IPNs are shown in Table I.

The densities of PU and PBMA homopolymers are 997 and 1055 $kg/m^3$ respectively. The density values of IPNs lie in the range 1044–1065 $kg/m^3$. The calculated densities were obtained by the volume additive principle which states that $[\rho = w_1\rho_1 + w_2\rho_2]$, where, $\rho$ is the density of the IPN sample, $w_1$ and $w_2$ are the weight fractions of the constituents, $\rho_1$ and $\rho_2$ are the corresponding densities respectively. From Table I, it was observed that, the densities of the IPNs are higher than that of corresponding homopolymers [25]. As the proportion of the PBMA homopolymer increased in the IPN, the density values increased correspondingly, since more and more dense PBMA was incorporated into the PU matrix. Disagreement of the actual and theoretical densities implies that there seems to be a high density crystalline region at the interface and/or high degree of hydrogen bond formation between PU and PBMA phases [26, 27]. The deviation between actual and theoretical densities is dependent on the degree of crosslinking and hydrogen bond formation at interpenetrated layers of PU and PBMA. This can also be explained by considering the fact that some of the holes in the comparatively loosely packed amorphous PU and PBMA structure, were filled up by the self-entanglement of the growing network [28].

Surface hardness reflects the resistance to local deformation, which is a complex property, related to crosslink density, modulus, strength, elasticity, plasticity and porosity of the polymer matrix. The surface hardness values of PU/PBMA lie in the range 83–90 Shore *A* and corresponding Shore *D* values are also given in Table I. These results lie in the expected range for cross linked IPNs. Resilience values of IPNs lie in the range 16–26. Resilience and surface hardness values of all IPNs are almost identical which may be due to the nature of both PU and PBMA are almost same.

The tensile strength of the IPNs lie in the range 3.0–5.50 MPa. However, the tensile strength value shows a maximum at about 60% BMA and then decreases with increase in BMA fraction [29, 30]. The small change in the properties below 50% BMA indicates that there is little intermixing between the two polymers and that BMA is dispersed in the PU continuous phase. A steep increase in properties at 60% PBMA content implies that the higher degree of physical entanglement and hydrogen bond formation between PU and PBMA network. This would result in an effective stress transfer between the two polymer components of the IPN upon deformation leading to an enhancement in the mechanical strength and retaining the percent elongation upon tensile deformation. The physical entanglement and hydrogen bond formation are most likely due to the formation of bicontinuous phase at a critical BMA composition. Such a transition has been reported previously for castor oil based PU/PS system [29, 31]. The critical second phase (BMA) concentration is also somewhat higher than reported previously by Susheela Bai *et al*. [29].

The tensile modulus of IPNs lie in the range 3.7–5.80 MPa. But there is no systematic variation in the tensile modulus value. The values of percentage elongation at break lie in the range 50–98% for IPNs (Table I). A slight fall in percentage elongation at break for IPN after incorporation of 20% BMA content indicates that there might be the formation of an intra-polyurethane network. Also, cross-linking and hydrogen bond formation take place between PU and PBMA chains. The grafting of the PBMA chains in this case would occur at the double bonds of the castor oil.

TABLE I Physico-mechanical properties of PU/PBMA IPNs

| Ratios of PU/PBM A (wt/wt, %) | Density ($kg/m^3$) | | Tensile strength (MPa) ±1% | %Elongation at break ±1% | Tensile modulus (MPa) ±2% | Surface hardness | | Resiliense |
|---|---|---|---|---|---|---|---|---|
| | Experimental ±2% | Theoretical | | | | Shore A ±2% | Shore D ±2% | |
| 80/20 | 1046 | 1008 | 3.8 | 55 | 5.5 | 90 | 48 | 26 |
| 60/40 | 1044 | 1020 | 3.3 | 66 | 5.8 | 88 | 39 | 19 |
| 50/50 | 1049 | 1026 | 3.0 | 50 | 5.0 | 83 | 35 | 18 |
| 40/60 | 1057 | 1031 | 5.5 | 78 | 3.7 | 86 | 39 | 16 |
| 20/80 | 1065 | 1043 | 4.1 | 98 | 3.9 | 88 | 40 | 19 |

TABLE II Optical properties of PU/PBMA IPNs

| Ratios of PU/PBMA (wt/wt, %) | Total percent transmittance | Total percent diffuse | Percent parallel | Percentage of haze |
|---|---|---|---|---|
| 80/20 | 70 | 17 | 52 | 20 |
| 60/40 | 70 | 5 | 65 | 12 |
| 50/50 | 69 | 12 | 57 | 23 |
| 40/60 | 72 | 5 | 67 | 15 |
| 20/80 | 77 | 11 | 65 | 10 |

## 3.3. Optical properties

The optical properties of thin IPN films have been carried out and the obtained results for total percent transmittance, total diffuse, percent parallel and haze values are given in Table II. These values are in the expected range [32]. From the table it was observed that all PU/PBMA IPNs are transparent films and their percent of transmittance is greater than 69.

Comparison of optical properties of 100% PU and 100% PBMA indicated that PBMA is a transparent film with 90% transmittance, while PU has 60% transmittance. PU films percent transmittance depends on the levels of NCO/OH ratio [32]. From Table II it was noticed that percent transmittance of IPN increases with increase in PBMA content. Thus IPNs containing low PU content are good transparent films with minimum haze value. From Table II, it was also noticed that, there were no systematic variation in haze values with PBMA content. This is due to the complicated chemical structure and morphology of the IPNs. Also crystalline size/amount and ratio between hard and soft segments of PUs affect the optical properties.

## 3.4. TGA studies

Typical TGA and its derivative thermogram of PU/PBMA (50/50) IPN are shown in Fig. 2. The thermograms obtained during TGA scans were analyzed to give the percent weight loss as a function of temperature. $T_0$ (temperature of onset decomposition), $T_{10}$ (temperature for 10% weight loss), $T_{20}$ (temperature for 20% weight loss) and $T_{50}$ (temperature for 50% weight loss) are the main criteria to indicate the heat stability of the IPNs. The higher the values of $T_0$, $T_{10}$, $T_{20}$ and $T_{50}$, the higher will be the heat stability of the IPNs. The integral procedural decomposition temperature (IPDT), which is an index of thermal stability, was determined using the method reported by Doyle [15]. The relative thermal stability of PU/PBMA IPNs were evaluated by comparing decomposition temperatures at various percent weight loss and IPDT values (Table III). From Table III, it can be seen that all the IPNs show same thermal degradation trend. IPDT values slightly decrease with increase in PBMA content. This is due to decrease in nitrogen content with increasing PBMA content in the IPNs. The IPDT values of all IPNs lie in the range 487–530°C. It is also seen from Table III that the OI values are very low and almost the same for all IPNs and lie in the range 0.12–0.30. Based upon the mass of carbonaceous char, it is concluded that IPNs are not good flame retardants as evidenced by their OI's [33].

The TGA thermogram of PU/PBMA IPNs shows three significant thermal degradation steps at 321, 378 and 466°C ($T_{max}$) for first, second and third steps (Table IV) respectively. The temperature range of decomposition, the percentage weight loss and percent of ash for each thermal degradation step are given in Table IV for all the PU/PBMA IPNs. From Table IV, it was observed that there was no systematic variation in weight loss with respect to PBMA composition. This may be due to the following reasons; (i) complicated chemical structure and morphology of the IPNs and (ii) the degree of hydrogen-bond formation between the carbonyl group of PBMA and —NH

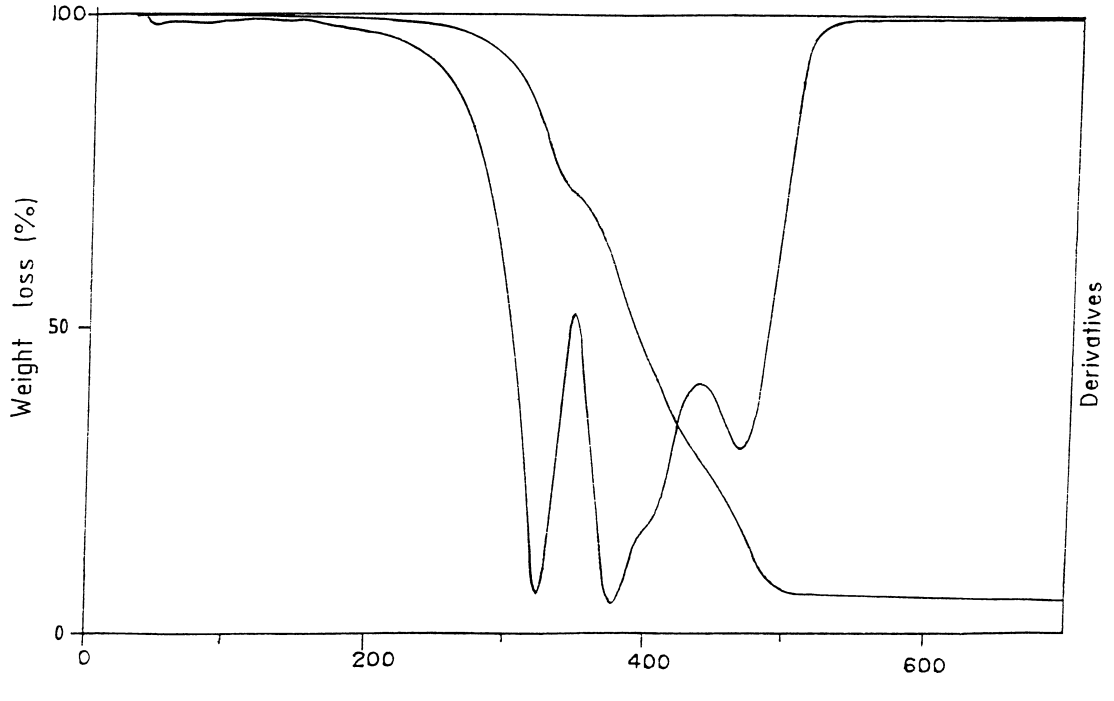


*Figure 2* TGA and DTG curve of 50/50 PU/PBMA IPN.

TABLE III Data obtained from TGA scans for PU/PBMA IPNs

| Composition of PU/PBMA (wt/wt, %) | Transition temperature (°C) upto various wt. loss ±2% | | | | IPDT values (°C) ±2% | O.I values |
|---|---|---|---|---|---|---|
| | $T_0$ | $T_{10}$ | $T_{20}$ | $T_{50}$ | | |
| 80/20 | 210 | 293 | 314 | 382 | 524 | 0.12 |
| 60/40 | 210 | 289 | 311 | 379 | 530 | 0.29 |
| 50/50 | 218 | 300 | 323 | 389 | 500 | 0.29 |
| 40/60 | 225 | 291 | 318 | 386 | 487 | 0.30 |
| 20/80 | 220 | 296 | 318 | 388 | 518 | 0.29 |

TABLE IV Data obtained from TGA scans of PU/PBMA IPNs

| Composition of PU/PBMA (wt/wt, %) | Process | Temperature range (°C) ±2 | | | Weight loss (%) |
|---|---|---|---|---|---|
| | | $T_0$ | $T_{max}$ | $T_c$ | |
| 80/20 | 1 | 207 | 317 | 343 | 29.2 |
| | 2 | 343 | 375 | 443 | 45.8 |
| | 3 | 443 | 463 | 521 | 23.3 |
| | Ash | – | – | – | 1.7 |
| 60/40 | 1 | 204 | 314 | 336 | 29.2 |
| | 2 | 336 | 372 | 429 | 45.0 |
| | 3 | 429 | 466 | 529 | 21.6 |
| | Ash | – | – | – | 4.2 |
| 50/50 | 1 | 218 | 321 | 346 | 29.2 |
| | 2 | 346 | 378 | 439 | 45.0 |
| | 3 | 439 | 466 | 507 | 21.6 |
| | Ash | – | – | – | 4.2 |
| 40/60 | 1 | 225 | 319 | 339 | 25.0 |
| | 2 | 339 | 376 | 443 | 32.5 |
| | 3 | 443 | 467 | 523 | 38.2 |
| | Ash | – | – | – | 4.3 |
| 20/80 | 1 | 220 | 316 | 339 | 27.5 |
| | 2 | 339 | 374 | 438 | 45.0 |
| | 3 | 438 | 466 | 521 | 23.4 |
| | Ash | – | – | – | 4.1 |

(urethane) group of PU is different for the different IPNs.

Generally the IPNs under observation do not break down in a simple manner, an individual sigmoid should be 100%, and there is a change in the morphological structure of the IPNs at each and every instant of pyrolysis, that affects the rate of decomposition. The first step weight loss occurs in the temperature range 204–346°C, which is due to loosely bound water molecules, oligomers, solvents, low molecular weight homopolymers, etc., with a mass loss of 25.0–29.2%. The weight loss that occurs in the second step in the temperature range 336–443°C, represents the mass loss of homopolymers with a loss of weight in the range 32.5–45.8%. The last and final step weight loss occurs in the range 429–529°C indicating the de-crosslinking and degradation of the IPN skeleton with a mass loss of 21.6–38.2%, all the IPNs having almost same ash content of about (∼4.2%) except 80/20 PU/PBMA systems. The formation of ash content is due to pyrolysed fragments of urethane linkage acting as a radical scavenger, which masks the rate of burning [34–37].

## 3.5. X-ray profile analysis

X-ray diffractrograms of 20/80, 50/50 and 80/20 PU/PBMA IPNs are shown in Fig. 3a–c. All the diffractrograms show one intense and broad peak at 22.89° ($2\theta$) which represents the prominent (110) reflection of IPNs. Further decrease in PBMA content decreases the peak intensity at 22.7° ($2\theta$). An additional intense peak around 12° ($2\theta$) was observed for 20/80 PU/PBMA IPN. This is due to the formation of dendrite structure in 20/80 PU/PBMA system. This peak disappears with

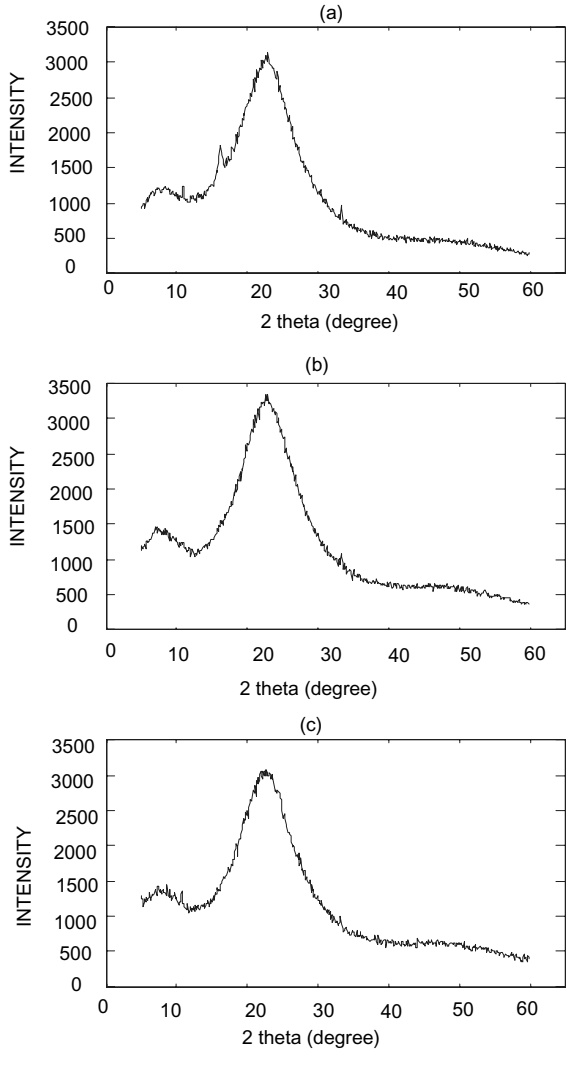


*Figure 3* X-ray diffraction patterns of PU/PBMA IPNs: (a) 20/80, (b) 50/50 and (c) 80/20.

TABLE V Microstructural parameters obtained from WAXS

| Composition of PU/PBMA IPNs (wt/wt, %) | $2\theta(^\circ)$ | $\langle N\rangle$ | p | $\alpha$ | $g$ (%) | $\alpha^*$ | $D_s$ (nm) | $d_{hkl}$ (nm) |
|---|---|---|---|---|---|---|---|---|
| 20/80 | 22.89 | $2.98 \pm 0.26$ | 2.58 | 2.45 | $1.5 \pm 0.1$ | 0.02 | 1.34 | 0.44 |
| 50/50 | 22.89 | $2.71 \pm 0.20$ | 1.87 | 1.20 | $3.0 \pm 0.2$ | 0.05 | 1.22 | 0.44 |
| 80/20 | 22.70 | $2.59 \pm 0.18$ | 1.75 | 1.18 | $1.5 \pm 0.1$ | 0.02 | 1.18 | 0.45 |

increase in PU content. This result is also supported by SEM studies.

It is evident from Fig. 3 that there is a broadening of the reflection, which arises due to two main factors. According to Warren [38] these are due to (i) decreasing in crystal size $\langle N\rangle$ and (ii) increase in strain (lattice disorder) ($g$ in%) present in the samples. These two microdefects are responsible for the broadening of the X-ray reflection in polymers. The number of unit cells (crystal size, $\langle N\rangle$) counted in a direction perpendicular to the Bragg plane is very small, of the order of 3 units or less in all IPNs. Along with this, there is also a lattice disorder of the second kind, known as paracrystallinity and normally this is quantified as strain ($g = \Delta d/d$). Profile analysis of these samples were carried out using the method proposed by Somashekar and Somashekarappa [21].

For the sake of completeness we have reproduced in Fig. 4a–c the simulated and experimental profile for PU/PBMA (20/80, 50/50 and 80/20) IPNs. In fact the goodness of the fit was better than 2% in all the IPNs which shows the models used here are quite reliable.

Table V gives the various microcrystalline parameters, including depth of crystal in terms of number of unit cells $\langle N\rangle$, width of the crystal size distribution ($\alpha$), the smallest crystal unit (p), lattice disorder ($g$) and the enthalpy ($\alpha^*$) of PU/PBMA IPNs. Table V also contains surface weighted crystal size ($D_s$) obtained by Fourier and simulation method for different compositions of IPNs. The order of magnitude of the surface weighted crystal size clearly indicates the extent of crystallinity present in the surface. From Table V it is evident that the microcrystalline parameters $\langle N\rangle$, p, $\alpha$ and $D_s$ values decrease with increase in PBMA content in the IPN matrix. This decrease in the microstructural parameters is due to decrease in crystal size, which is due to molecular organizational changes in the IPNs. From the $\langle N\rangle$ and $g$ parameters, the enthalpy ($\alpha^*$) was calculated using Hosemann's paracrystalline disorder model [39].

Where,

$$\alpha^* = \langle N\rangle^{1/2} g \tag{7}$$

Here, enthalpy ($\alpha^*$) physically means that the growth of paracrystals in a particular material is appreciably controlled by the level of $g$ in the net plane structure. The phase stabilization occurs in all IPNs. This conclusion has been made on the basis of minimum value of $\alpha^*$ (0.02–0.05), the enthalpy which is a measure of the energy required for the formation of net plane structure.

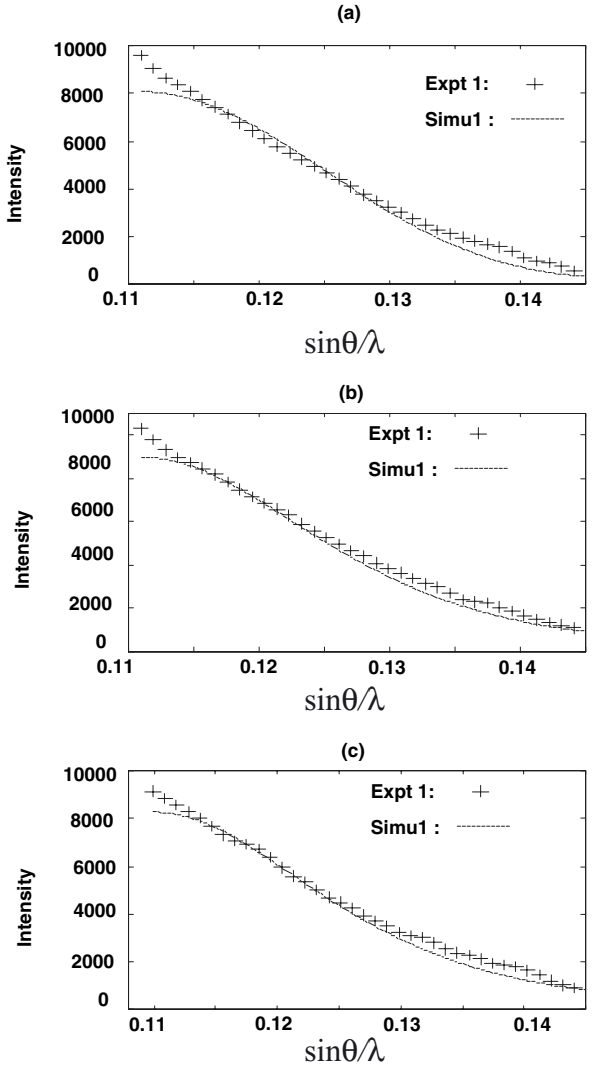


*Figure 4* Experimental and simulated profiles of PU/PBMA IPNs: (a) 20/80, (b) 50/50 and (c) 80/20.

## 3.6. Scanning electron microscopy (SEM)

SEM microphotographs for 20/80, 60/40 and 40/60 PU/PBMA IPNs are shown in Fig. 5a–c respectively. From Fig. 5a it was noticed that growth of dendrites occurred; this might be due to crystallization of PBMA homopolymer in PU. The crystalline super structure disappears with increase in PU composition in IPNs. From Fig. 5b and c it was noticed that two-phase morphology for 60/40 and 40/60 PU/PBMA IPNs and an uniform distribution of second component. A slight different surface texture was noticed in 60/40 and 40/60 (Fig. 5b and c) systems. This result reveals the two phase morphology of IPNs.

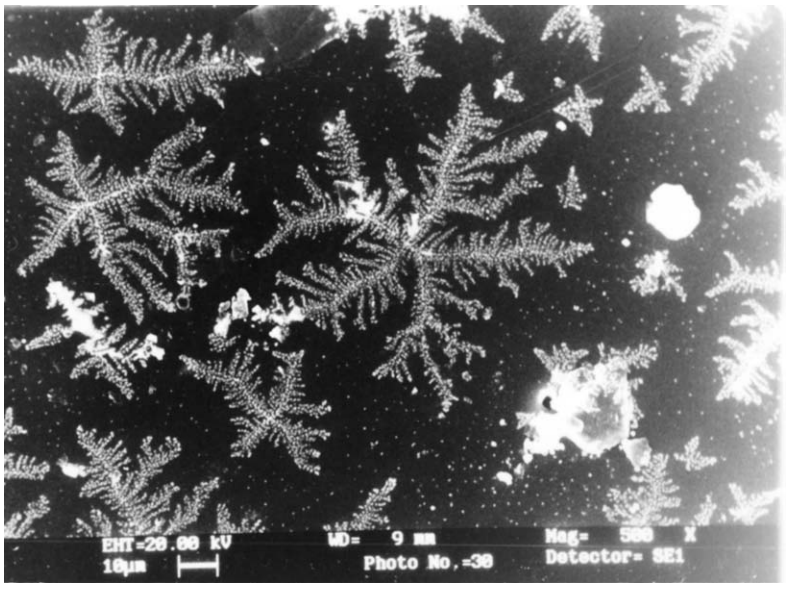


(a)

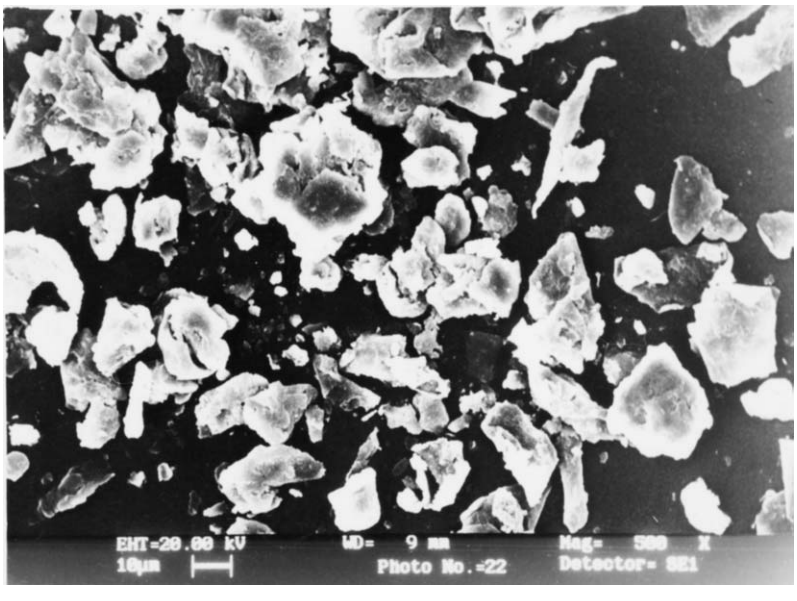


(b)

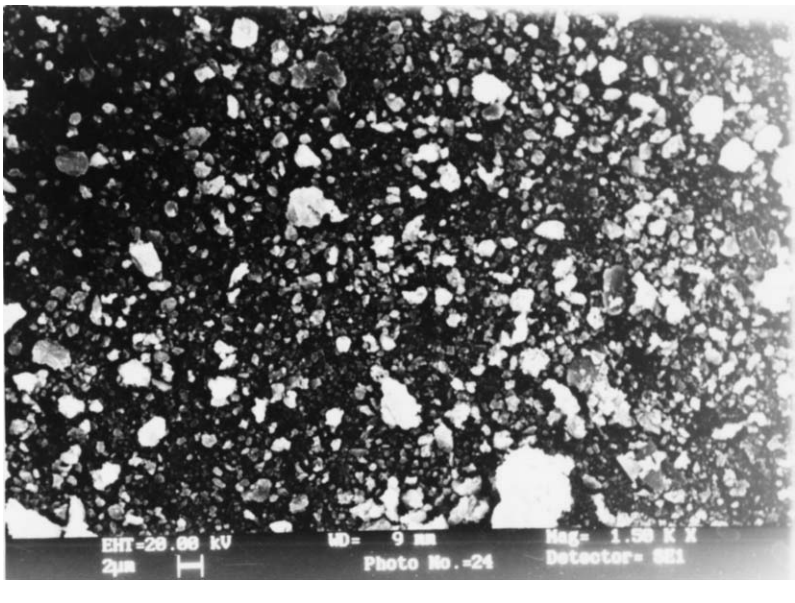


(c)

*Figure 5* Scanning electron micrographs of PU/PBMA IPNs: (a) 20/80, (b) 60/40 and (c) 40/60.

## 4. Conclusions

The following conclusions can be drawn from the present investigation:

1. From FTIR spectra, it was confirmed that hydrogen bond formation between the PU and PBMA networks.

2. The highest tensile properties were observed for 40/60 PU/PBMA IPN, indicating that 40/60 is in the critical composition.

3. Variation in percent transmittance is due to change in the composition of IPN.

4. From TGA thermograms it was noticed that all the IPNs are stable up to 210°C and maximum degradation takes place beyond 507°C.

5. TGA curves of IPNs show three significant thermal degradation steps in the temperature range 204–346, 336–443 and 429–529°C for first, second and third steps respectively. Thermal decomposition of IPNs is complicated because IPNs have complicated chemical structure.

6. The phase stabilization occurs for all IPNs. This conclusion has been arrived on the basis of the minimum value of $\alpha^*$.

7. The physical properties like tensile strength and percentage elongation at break show a marked improvement when crystal size $\langle N \rangle$ and $D_S$ values are in between maximum and minimum.

8. SEM micrographs reveals dendritic growth for 20/80 PU/PBMA IPN and two phase morphology for the other IPNs.

## References


1. G. M. ESTES, S. L. COOPER and A. V. TOBOLSKY, *J. Macromol. Sci. Rev. Macromol. Chem.* **4** (1970) 313.
2. J. W. C. VAN BOGART, P. E. GIBSON and S. L. COOPER, *J. Polym. Sci. Polym. Phys. Ed.* **21** (1983) 65.
3. J. OPHIR and G. L. WILKES, *ibid.* **18** (1980) 1969.
4. L. W. BARRETT and L. H. SPERLING, *Polym. Engng. Sci.* **33**(14) (1993) 913.
5. L. H. SPERLING, "Interpenetrating Polymer Networks and Related Materials"(Plenum, New York, 1981).
6. *Idem.*, *Macromol. Rev.* **12** (1977) 141.
7. L. H. SPERLING, J. A. MANSON and M. A. LINNE, *J. Polym. Mater.* **1** (1984) 54.
8. R. E. TOUHSAENT, D. A. THOMAS and L. H. SPERLING, *J. Polym. Mater. Sci.*; Part C **46** (1974) 75.
9. N. DEVIA, J. A. MANSON, L. H. SPERLING and A. CONDE, *Polym. Engng. Sci.* **18**(3) (1978) 200.
10. L. H. SPERLING and J. M. WIDMAIER, *Polym. Engng. Sci.* **23** (1983) 693.
11. SIDDARAMAIAH, P. MALLU and R. SOMASHEKAR, *J. Appl. Polym. Sci.* **68** (1998) 1739.
12. P. MALLU, SIDDARAMAIAH and R. SOMASHEKAR, *Bull. Matl. Sci.* **23**(5) (2000) 413.
13. T. JEEVANANDA, MUNEERA BEGUM and SIDDARAMAIAH, *Eur. Polym. J.* **37**(6) (2001) 1213.
14. P. PATEL, T. SHAH and B. SUTHAR, *J. Polym. Mater.* **6** (1989) 193.
15. C. D. DOYLE, *Anal. Chem.* **33** (1961) 77.
16. A. R. STOKES, *Proc. Phys. Soc. London* **61** (1948) 382.
17. A. J. C. WILSON, "Elements of X-ray Crystallography" (Addison Wesley, Reading, MA, 1970) Vol. 191.
18. W. PRESS, B. P. FLANNERY, S. TENKOLSLEY and W. T. VELTERLING (ed.), "Numerical Recipes" (Cambridge Univ. Press, UK, 1986) vol. 83.
19. MARK SILVER, M.Sc., Thesis, UMIST, UK (1998).
20. D. BALZAR, *J. Res. Nat. Inst. Stand. Tech.* **88** (1993) 32.
21. R. SOMASHEKAR and H. SOMASHEKARAPPA, *J. Appl. Cryst.* **30** (1997) 147.
22. D. DAS, S. S. NAYAK, S. K. DAS, P. L. NAYAK and S. LENKA, *Thermo Chimica Acta* **297** (1997) 101.
23. G. S. PATHIS, M. NIAOUNAKIS, E. KONTOU, L. APEKIS, P. PISSIS and C. CHRISTODOULIDES, *J. Appl. Polym. Sci.* **54** (1994) 831.
24. R. W. SEYMOUR, G. M. ESTERS and S. L. COOPER, *Macromolecules* **3** (1970) 579.
25. S. RAUT and V. ATHAWALE, *Eur. Polym. J.* **36** (2000) 1379.
26. H. DJOMO, A. MARIN, M. AMYANIDU and G. MAYER, *Polymer* **24** (1983) 65.
27. V. CHOUDHARY and R. GUPTA, *J. Appl. Polym. Sci.* **50** (1963) 1075.
28. R. MILLAR, *J. Chem. Soc.* **1311** (1960).
29. SUSHEELA BAI, D. V. KHAKHAR and V. N. NADKARNI, *J. Polym. Sci.* **38** (1997) 1319.
30. B. SUTHAR, N. PARIKH and N. PATEL, *Polym. Intl.* **25** (1991) 175.
31. W.-H. KU, J.-L. LIANG, K.-T. WEI, H.-T. LIU, C.-S. HUANG, S.-Y. FANG and W.-G. WU, *Macromolecules* **24** (1991) 4605.
32. YU. S. LIPATOV, V. V SHILOV, YUP. GOMZA, V. S. SKORODZIEVSKY, A. I. USTINOV and K.V. TCHUISSTOV, *Polymer* **25** 459 (1984).
33. D. PARIDA, S. LENKA and P. L. NAYAK, *J. Macro. Sci., Pure Appl. Chem* **A 32**(7) (1995) 1365.
34. SIDDARAMAIAH, P. MALLU and A. VARADARAJULU, *Polym. Degrad. Stab.* **63** (1999) 305.
35. R. N. SANTRA, P. G. MUKUNDA, G. B. NANDO and T. K. CHAKI, *Thermochimica Acta* **219** (1993) 283.
36. P. D. NAIR and M. JAYABALAN, *J. Polym. Sci., Polym. Chem. Ed.* **28** (1990) 3775.
37. K. WANG, C. LUO and X. M. ZHOU "Analytical Technique on Polymers" (Qinhua Uni. Press, Beijing, People's Republic of China, 1991).
38. B. E. WARREN and B. L. AVERBACH, *J. Appl. Phys.* **21** (1950) 595.
39. R. HOSEMANN, *Prog. Coll. Polym. Sci.* **77** (1988) 15.



*Received 3 September 2002*
*and accepted 15 January 2004*